Steel and Composite Structures, *Vol. 29, No. 3 (2018) 379-389*
DOI: https://doi.org/10.12989/scs.2018.29.3.379

Buckling analysis of elastically-restrained steel plates under eccentric compression

Ying Qin [*1,2], Gan-Ping Shu [1], Er-Feng Du [1] and Rui-Hua Lu [1]

[1] *Key Laboratory of Concrete and Prestressed Concrete Structures of Ministry of Education, and National Prestress Engineering Research Center, School of Civil Engineering, Southeast University, Nanjing, China*
[2] *State Key Laboratory of Subtropical Building Science, South China University of Technology, Guangzhou, China*

(*Received May 27, 2018, Revised September 30, 2018, Accepted October 23, 2018*)

Abstract. In this research, the explicit closed-form local buckling solution of steel plates in contact with concrete, with both loaded and unloaded edges elastically restrained against rotation and subjected to eccentric compression is presented. The Rayleigh-Rize approach is applied to establish the eigenvalue problem for the local buckling performance. Buckling shape which combines trigonometric and biquadratic functions is introduced according to that used by Qin *et al.* (2017) on steel plate buckling under uniform compression. Explicit solutions for predicting the local buckling stress of steel plate are obtained in terms of the rotational stiffness. Based on different boundary conditions, simply yet explicit local buckling solutions are discussed in details. The proposed formulas are validated against previous research and finite element results. The influences of the loading stress gradient parameter, the aspect ratio, and the rotational stiffness on the local buckling stress resultants of steel plates with different boundary conditions were evaluated. This work can be considered as an alternative to apply a different buckling shape function to study the buckling problem of steel plate under eccentric compression comparing to the work by Qin *et al*. (2018), and the results are found to be in consistent with those in Qin *et al*. (2018).

Keywords: explicit analysis; local buckling; rotationally restrained; combined compression and bending; steel plate

1. Introduction

Concrete-filled tubular (CFT) columns are used increasingly in many engineering fields. Due to the availability of high strength materials, thin-walled steel tubes are becoming more popular (Qin *et al.* 2016). The relatively low stiffness of thin-walled tube leads to the local instability of steel plate when subjected to combined bending and compression (Liu *et al.* 2018). Meanwhile, square steel tubes are increasingly used as bracings in earthquakes-resisting structures. The buckling in the compression range of the bracing significantly reduces the energy dissipating capacity of the structures. Infill materials like concrete may be used as filler to form the buckling restrained braces, which prevent the buckling of steel plate inwards and thus, improve the structural behavior (Gheidi *et al.* 2011, Mirtaheri *et al.* 2018). Furthermore, progressive collapse, which causes significant loss of property and life, has been one of the most important issues in civil engineering and has been interested by civil engineers. Local buckling of structural members may be distributed through entire structure and lead to progressive collapse (Mirtaheri and Zoghi 2016). Therefore, the consideration for local buckling is essential for efficient and reliable design of different structural components. In general, the investigation on local buckling of steel tube is conducted by modelling the web plate and flange plate individually and considering the adjacent plates as boundary supports. In this way, each component is modelled as a steel plate with different boundary conditions and subjected to combined bending and compression.

A number of research have been conducted on the local buckling of plates under different loadings and with varying edge restraints. Qiao *et al.* (2013) studied the case of composite plate with two opposite edges simply-supported and the other two opposite edges either both rotationally restrained or one rotationally restrained and the other free and subjected to combined linearly varying axial and in-plane shear loading. Villarreal and Abajo (2018) described a theoretical approach for the buckling analysis of rotationally restrained orthotropic plates. Recently, Klouche *et al.* (2017) and Dong *et al.* (2017) proposed an analytical method to obtain the shear buckling coefficient of thick isotropic plate and symmetrically laminated composite plate, respectively. Liu *et al.* (2017) studied the local buckling behavior of extreme thick-walled cold-formed square steel tube. Abbasi *et al.* (2018) used compound strip method to the buckling analysis of steel with discrete fasteners. Burgos *et al.* (2018) focused on the buckling of horizontal steel tanks supported on discrete saddles under pressure. Yerudkar and Vesmawala (2018) investigated the buckling performance of cold-formed steel laterally braced stiffened C and Z section members under combined bending and torsion.

Meanwhile, the plate contact buckling theory has been studied by some researchers. De Holanda and Gonçalves

*Corresponding author, Ph.D., Professor,
E-mail: qinying@seu.edu.cn

ISSN: 1229-9367 (Print), 1598-6233 (Online)

(2003) investigated the buckling and large deflection post-buckling performance of plates laterally constrained by a tensionless foundation and subjected to in-plane compressive forces. Shen and Li (2004) studied the post-buckling responses of shear deformable laminated plates supported by a tensionless elastic foundation and under in-plane compressive edge loads or a uniform temperature rise. Li *et al*. (2016) evaluated the end condition effect through the buckling analysis of finite length plates with various boundary conditions resting on an elastic foundation. Naghsh *et al*. (2018) performed thermal buckling analysis of point-supported thin laminated composite plates. Dong *et al*. (2018) investigated the buckling performance of a long thin orthotropic plate on a tensionless rigid foundation under combined in-plane shear and bending.

In contrast to extensive research on the closed-formed exact solutions for the local buckling of steel plates, most studies on local buckling of steel plates in contact with concrete are based on numerical approaches. Uy and Bradford (1996) used a finite strip method to evaluate the elastic local buckling performance of steel plates in composite steel-concrete members. Patton and Singh (2017) investigated the buckling behavior of fixed-ended concrete-filled tubular columns through finite element analysis.

Furthermore, closed-formed exact solutions for the local buckling of steel plates in contact with concrete are quite limited. Long *et al*. (2016) investigated the local buckling of steel plates in concrete-filled steel tubular columns subjected to eccentric compression and with clamped loaded edges. Qin *et al*. (2017) provided analytical solutions for the critical buckling stress for steel plates in concrete-filled tubular columns subjected to uniform compression and with elastically-restrained four edges. The shape function was constructed by a combine sine and cosine function in the x direction and a biquadratic function in the y direction. In addition, Qin *et al*. (2018) studied the buckling of steel plates in composite structures under combined bending and compression with the buckling shape function of combined sinusoidal and cosine functions along both x- and y-directions. The research in this paper can be regarded as an extension to work by Qin *et al*. (2017) to employ the buckling shape in Qin *et al*. (2017) to the case of steel plates under eccentric compression and an alternative to study in Qin *et al*. (2018) by applying a different buckling shape function.

For a CFT column in real project, it generally bears both axial compression and bending moment, as shown in Fig. 1. The pure compression plus pure bending on the steel plate can be considered as eccentric compression. The four edges of the steel plate are restrained against rotation, to some extent, by the adjacent plates.

As the boundary condition of steel plate is largely determined by the stiffness of adjacent plate field, it is expected that the four edges of the steel plate in CFT column is restrained from rotation by the adjacent plate fields and infilled concrete. However, the degree of restraint is not complete since the steel plate fields are normally not stiff enough to form the clamped boundary. Therefore, it is more appropriate to assume the steel plates are elastically restrained along both loaded and unloaded edges (Qin *et al*. 2017, 2018). For steel plates with this more realistic boundary conditions, the local buckling problem can be solved by the finite element method (Thai *et al*. 2017, Fang *et al*. 2017). Although the finite element techniques are capable of capturing a variety of nonclassical cases with various degree of flexibility along the steel plate edges, it is time consuming and tedious for general use by structural engineers.

In this research, the buckling shape function, which was proposed by Qin *et al*. (2017) to study the case of steel plate under uniform compression, was introduced to reflect the steel plate in rigid contact with concrete while elastically restrained along four edges. Furthermore, the hand calculation method for steel plate under eccentric compression was derived to exclude the needs for complicated numerical simulations as used by previous research.

The formulation of energy method is first presented, followed by explicitly capturing the critical local buckling load under combined bending and compression using the Rayleigh-Ritz method, which resembles the methods by Qin *et al*. (2017) and Qin *et al*. (2018). The buckling shape function for the elastically restrained steel plates is constructed by combining trigonometric and biquadratic functions as used by Qin *et al*. (2017). Several special cases are simplified from the general solutions, and their local buckling coefficients are compared with both the available solutions and the finite element eigenvalue solutions, thus validating the accuracy of the proposed explicit analytical formulas. A parametric study is then conducted to evaluate the effects of the loading stress gradient parameter, the

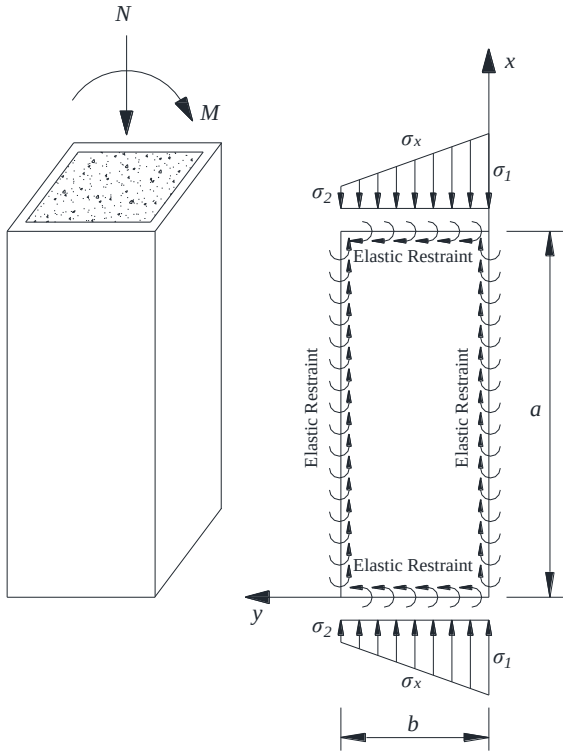

Fig. 1 Elastically restrained steel plates under combined bending and compression

aspect ratio, and the rotational restraint stiffness on the local buckling stress of elastically restrained steel plates. This work can be considered as the effort to use a different buckling shape function comparing to that in Qin *et al*. (2018) to investigate the local buckling of steel plate in composite structures under eccentric compression.

2. Analytical formulation

2.1 Formulation for elastically-restrained steel plates

This section offers the basic formulation for steel plates with elastic restraint along four edges. It should be noted that the knowledge in this section can be found in many textbooks regarding plate buckling or in references such as Qiao *et al*. (2013), Qin *et al*. (2017, 2018), and Dong *et al*. (2018). The brief formulation was provided below for the readers' convenience and the readers could refer to the references mentioned above for detailed information.

The total potential energy of the steel plate system Π is given as Eq. (1).

$$\Pi = U + V + U_{\Gamma} \tag{1}$$

where U is the elastic strain energy stored in the deformed steel plate as given by Eq. (2); U_{Γ} is the restraining energy stored in the rotational springs along the loaded and unloaded edges as shown in Eq. (4), V is the work done by the external bending and compression as expressed by Eq. (5).

$$U = \frac{D}{2}\iint_{W}\left\{\begin{array}{l}\left(\frac{\partial^2 w}{\partial x^2}+\frac{\partial^2 w}{\partial y^2}\right)^2 - 2(1-\nu) \\ \left[\frac{\partial^2 w}{\partial x^2}\frac{\partial^2 w}{\partial y^2} - \left(\frac{\partial^2 w}{\partial x \partial y}\right)^2\right]\end{array}\right\} dxdy \tag{2}$$

$$D = \frac{Et^3}{12\left(1-\nu^2\right)} \tag{3}$$

$$\begin{aligned} U_{\Gamma} = {} & \frac{1}{2}\int_{\Gamma x} k_y \left(\frac{\partial w}{\partial y}\Big|_{y=0}\right)^2 dx + \frac{1}{2}\int_{\Gamma x} k_y \left(\frac{\partial w}{\partial y}\Big|_{y=b}\right)^2 dx \\ & + \frac{1}{2}\int_{\Gamma y} k_x \left(\frac{\partial w}{\partial x}\Big|_{x=0}\right)^2 dy + \frac{1}{2}\int_{\Gamma y} k_x \left(\frac{\partial w}{\partial x}\Big|_{x=a}\right)^2 dy \end{aligned} \tag{4}$$

$$V = \frac{1}{2}\iint_{W} N_x \left(\frac{\partial w}{\partial x}\right)^2 dxdy \tag{5}$$

where W is the area of the steel plate; v is the Poisson's ratio and can be taken as 0.3; w is the buckling shape for the steel plate; E is the elastic modulus of steel; t is the thickness of steel plate; k_x, k_y are the elastic rotational stiffness of springs at the loaded edges and unloaded edges, respectively; Γ_x, Γ_y are the boundary lines along the unloaded edges ($y = 0$ and $y = a$) and loaded edges ($x = 0$ and $x = b$), respectively; $N_x = \sigma_x t$ is the axial load per unit length at the boundary line along the loaded edges. The stress distribution along the x-direction is shown in Fig. 1 and can be given by Eq. (6).

$$\sigma_x = \sigma_1\left(1 - \varsigma\frac{y}{b}\right) \tag{6}$$

where ς is the loading stress gradient parameter along the y-direction and is given by Eq. (7). It should be noted that $0 < \varsigma < 1$ represents the case that the steel plate is under combined in-plane bending and compression, as the plate is subjected to linearly varying axial edge loads.

$$\varsigma = \frac{\sigma_1 - \sigma_2}{\sigma_1} \tag{7}$$

By choosing the appropriate out-of-displacement buckling shape and substituting it into Eqs. (2), (4), and (5) and the corresponding results into Eq. (1), the buckling eigenvalue problem can be obtained by Rayleigh-Rize method.

2.2 Buckling shape for the plate

An adequate approach for the out-of-plane buckling shape function w should satisfy both boundary and load conditions. For steel plate elastically restrained against rotation at both loaded and unloaded edges, the boundary conditions should meet the requirements given by Eq. (8) (Qin *et al*. 2017, 2018).

$$w(0,y) = w(a,y) = 0 \tag{8a}$$

$$M_x(0,y) = -D\left(\frac{\partial^2 w}{\partial x^2}\right)_{x=0} = -k_x\left(\frac{\partial w}{\partial x}\right)_{x=0} \tag{8b}$$

$$M_x(a,y) = -D\left(\frac{\partial^2 w}{\partial x^2}\right)_{x=a} = +k_x\left(\frac{\partial w}{\partial x}\right)_{x=a} \tag{8c}$$

$$w(x,0) = w(x,b) = 0 \tag{8d}$$

$$M_y(x,0) = -D\left(\frac{\partial^2 w}{\partial y^2}\right)_{y=0} = -k_y\left(\frac{\partial w}{\partial y}\right)_{y=0} \tag{8e}$$

$$M_y(x,b) = -D\left(\frac{\partial^2 w}{\partial y^2}\right)_{y=b} = +k_y\left(\frac{\partial w}{\partial y}\right)_{y=b} \tag{8f}$$

On the other hand, for steel plate in contact with concrete, the plate can only buckle outwards. This means the value of w should be no less than zero in any cases. Furthermore, due to the applied loading of eccentric compression at $x = 0$ and $x = a$, the buckling shape should exhibit the symmetry properties about straight line $x = 0.5a$ while show the asymmetry behavior about $y = 0.5b$.

In CFT columns, the infilled concrete is regarded as the rigid material to be in contact with the steel plate (Wright 1993). Therefore, the steel plate can be considered to be resting on a rigid foundation. According to the research by Ma *et al*. (2008), a single half-wave buckling model

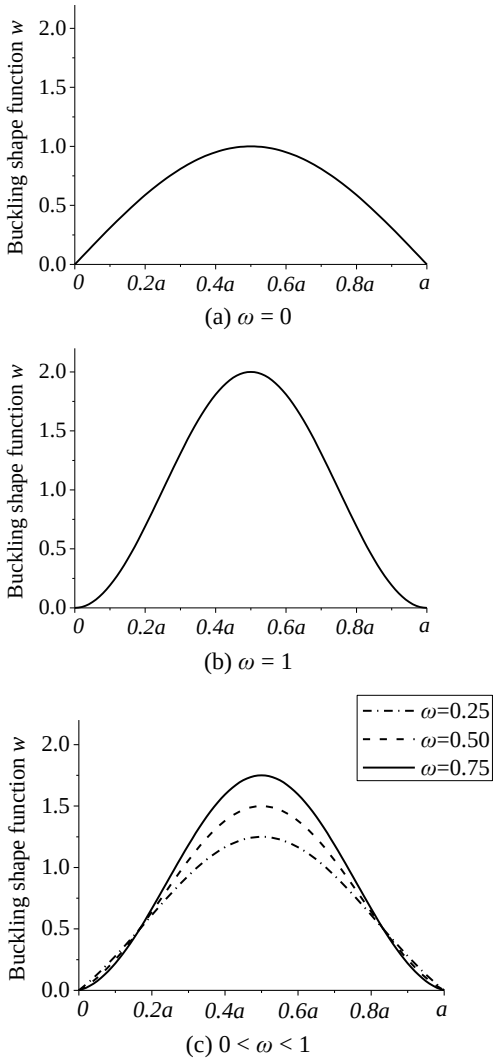

(a) $\omega = 0$

(b) $\omega = 1$

(c) $0 < \omega < 1$

Fig. 2 Buckling shapes with different ω values

along the *x*-direction is appropriate. Therefore, it is assumed that in the *x*-direction the combination of weighted sinusoidal function and cosine function describes the buckling shape, while in the *y*-direction a biquadratic function is applied, which can be expressed as Eq. (9). It should be noted that this type of shape function has been used by Qin *et al*. (2017) to deal with steel plate under uniform compression. The research in this paper extends the application of this equation to the case of steel plate under combined bending and compression. In addition, the buckling shape function with combined sinusoidal and cosine functions along both *x*- and *y*-directions has been used by Qin *et al*. (2018) to investigate the same problem. It will be seen from the discussion in Section 3 that, the application of buckling shape function in this research generates similar and consistent results to those by Qin *et al*. (2018), which indirectly verifies the accuracy of the used shape function.

It should also be noted that a double series of simple sin-functions along both *x* and *y* directions is commonly used by many researchers in previous studies. However, this generally-adopted function is too complicated with many unknown parameters to obtain the explicit solution. Furthermore, this function cannot meet the deformation requirement for steel plates in composite structures.

$$w(x,y) = C\left[(1-\omega)\sin\frac{\pi x}{a} + \omega\left(1-\cos\frac{2\pi x}{a}\right)\right] \times\left[\frac{y}{b} + \phi_1\left(\frac{y}{b}\right)^2 + \phi_2\left(\frac{y}{b}\right)^3 + \phi_3\left(\frac{y}{b}\right)^4\right] \tag{9}$$

where C is a constant, and ϕ_1, ϕ_2, ϕ_3 and ω are the constants to be determined which should satisfy both the boundary conditions and the requirement of compatibility. By choosing proper value of ω, the buckling function exhibits reasonable shape to reflect the elastic restraint along loaded edges, as shown in Fig. 2.

It can be observed that the shape function specified in Eq. (9) exactly satisfies the boundary conditions given in Eq. (8a). Substituting the first-order partial derivative and the second-order partial derivative of Eq. (9) with respect to *x* into Eq. (8b) or (8c) gives the weight constant ω in terms of the rotational stiffness of the elastic restraint (k_x) along the loaded edges

$$\omega = \frac{k_x a}{k_x a + 4\pi D} \tag{10}$$

Similarly, substituting the derivative function of Eq. (9) with respective to *y* into Eqs. (8d)-(8f), the unknown constants ϕ_1, ϕ_2, and ϕ_3 can be solved in terms of the elastic rotational restraint stiffness (k_y) along the two opposite unloaded edges as shown in Eq. (11).

It can be observed that the change in the loading condition from uniform compression in Qin *et al*. (2017) to eccentric compression in this research does not change the expression of ω, ϕ_1, ϕ_2, and ϕ_3.

$$\phi_1 = \frac{k_y b}{2D} \tag{11a}$$

$$\phi_2 = -2 - \frac{k_y b}{D} \tag{11b}$$

$$\phi_3 = 1 + \frac{k_y b}{2D} \tag{11c}$$

Substituting Eq. (9) into Eqs. (2), (4), and (5) and integrating gives Eqs. (12a)-(12c). The commercial software MATLAB was used to solve this problem for time-saving, though the mathematical derivation can be completed by hand calculation.

$$U = \frac{D}{2}\left[\frac{b\pi^3 C^2}{a^3}A_1B_1 + \frac{aC^2}{b^3}A_2B_2 + 2(1-\nu)\frac{\pi C^2}{ab}A_3B_3 - 2\nu\frac{\pi C^2}{ab}A_4B_4\right] \tag{12a}$$

$$U_G = \frac{k_y a C^2}{2b^2}\left(1 + A_6^2\right)B_5 + \frac{k_x b\pi^2 C^2 (1-\omega)^2}{a^2}A_7 \tag{12b}$$

$$V = -\frac{\sigma_1 tb\pi C^2}{2a}A_5B_4 \tag{12c}$$

where A_1, A_2, A_3, A_4, A_5, A_6, A_7, B_1, B_2, B_3, B_4, and B_5 are defined as

$$A_1 = \frac{1}{3} + \frac{\phi_1}{2} + \frac{\phi_3 + \phi_1\phi_2}{3} + \frac{\phi_2\phi_3}{4} + \frac{\phi_1^2 + 2\phi_2}{5} + \frac{\phi_2^2 + 2\phi_1\phi_3}{7} + \frac{\phi_3^2}{9} \tag{13a}$$

$$A_2 = 4\phi_1^2 + 12\phi_2^2 + \frac{144}{5}\phi_3^2 + 12\phi_1\phi_2 + 16\phi_1\phi_3 + 36\phi_2\phi_3 \tag{13b}$$

$$A_3 = 1 + 2\phi_1 + 2\phi_2 + 2\phi_3 + \frac{4}{3}\phi_1^2 + \frac{9}{5}\phi_2^2 + \frac{16}{7}\phi_3^2 + 3\phi_1\phi_2 + \frac{16}{5}\phi_1\phi_3 + 4\phi_2\phi_3 \tag{13c}$$

$$A_4 = \phi_1 + 2\phi_2 + 3\phi_3 + \frac{2}{3}\phi_1^2 + \frac{6}{5}\phi_2^2 + \frac{12}{7}\phi_3^2 + 2\phi_1\phi_2 + \frac{14}{5}\phi_1\phi_3 + 3\phi_2\phi_3 \tag{13d}$$

$$A_5 = -\left(\frac{1}{6}\phi_1^2 + \frac{2}{7}\phi_1\phi_2 + \frac{1}{4}\phi_1\phi_3 + \frac{2}{5}\phi_1 + \frac{1}{8}\phi_2^2 + \frac{2}{9}\phi_2\phi_3 + \frac{1}{3}\phi_2 + \frac{1}{10}\phi_3^2 + \frac{2}{7}\phi_3 + \frac{1}{4}\right)\varsigma + \frac{1}{3} + \frac{\phi_1}{2} + \frac{\phi_3 + \phi_1\phi_2}{3} + \frac{\phi_2\phi_3}{4} + \frac{\phi_1^2 + 2\phi_2}{5} + \frac{\phi_2^2 + 2\phi_1\phi_3}{7} + \frac{\phi_3^2}{9} \tag{13e}$$

$$A_6 = 1 + 2\phi_1 + 3\phi_2 + 4\phi_3 \tag{13f}$$

$$A_7 = \frac{1}{3} + \frac{1}{2}\phi_1 + \frac{2}{5}\phi_2 + \frac{1}{3}\phi_3 + \frac{1}{3}\phi_1\phi_2 + \frac{2}{7}\phi_1\phi_3 + \frac{1}{4}\phi_2\phi_3 + \frac{1}{5}\phi_1^2 + \frac{1}{7}\phi_2^2 + \frac{1}{9}\phi_3^2 \tag{13g}$$

$$B_1 = \frac{\pi(1-\omega)^2}{2} + 8\pi\omega^2 - \frac{16\omega(1-\omega)}{3} \tag{13h}$$

$$B_2 = \frac{(1-\omega)^2}{2} + \frac{3\omega^2}{2} + \frac{14\omega(1-\omega)}{3} \tag{13i}$$

$$B_3 = \frac{\pi(1-\omega)^2}{2} + 2\pi\omega^2 + \frac{8\omega(1-\omega)}{3} \tag{13j}$$

$$B_4 = \frac{\pi(1-\omega)^2}{2} + 2\pi\omega^2 + \frac{16\omega(1-\omega)}{3} \tag{13k}$$

$$B_5 = \frac{(1-\omega)^2}{2} + \frac{3\omega^2}{2} + \frac{4\omega(1-\omega)}{\pi} \tag{13l}$$

It can be observed that the main differences for equations between the cases of uniform compression in Qin *et al*. (2017) and eccentric compression in this research lie in the change of expression of V when comparing to Qin *et al*. (2017).

2.3 Explicit solution

The method to obtain the explicit solution of steel plate under eccentric compression assembles the methods used by Qin *et al*. (2017, 2018). Inserting Eqs. (12a)-(12c) into Eq. (1) leads to the following explicit expression for the total potential energy of the steel plate

$$P = \frac{D}{2}\left[\begin{array}{l}\frac{b\pi^3C^2}{a^3}A_1B_1 + \frac{aC^2}{b^3}A_2B_2 \\ +2(1-\nu)\frac{\pi C^2}{ab}A_3B_3 - 2\nu\frac{\pi C^2}{ab}A_4B_4\end{array}\right] - \frac{\sigma_1 tb\pi C^2}{2a}A_5B_4 + \frac{k_y aC^2}{2b^2}\left(1+A_6^2\right)B_5 + \frac{k_x b\pi^2C^2(1-\omega)^2}{a^2}A_7 \tag{14}$$

The fundamental relation that governs the buckling shape of the steel plate states that the first-order derivative of the potential energy P in the buckled state has to vanish

$$\frac{\partial P}{\partial C} = 0 \tag{15}$$

Inserting Eq. (14) into Eq. (15) and rearranging leads to the following governing equation for the critical buckling stress

$$\sigma_x t = \frac{\pi^2 D}{b^2}\left[\begin{array}{l}\frac{A_1B_1}{\gamma^2A_5B_4} + \frac{\gamma^2A_2B_2}{\pi^3A_5B_4} \\ +\frac{2(1-\nu)A_3B_3 - 2\nu A_4B_4}{\pi^2A_5B_4} \\ +\frac{2\lambda_y\gamma^2\left(1+A_6^2\right)B_5}{\pi^3A_5B_4} + \frac{4\lambda_x(1-\omega)^2A_7}{\gamma^2\pi A_5B_4}\end{array}\right] = \frac{k\pi^2D}{b^2} \tag{16}$$

where γ is the aspect ratio and is defined as $\gamma = a/b$; k is the elastic local buckling coefficient of the steel plate as given in Eq. (17); λ_x and λ_y are the elastically restraining factors of loaded and unloaded edges, respectively, as defined in Eqs. (18a)-(18b).

$$k = \frac{A_1B_1}{\gamma^2A_5B_4} + \frac{\gamma^2A_2B_2}{\pi^3A_5B_4} + \frac{2(1-\nu)A_3B_3 - 2\nu A_4B_4}{\pi^2A_5B_4} + \frac{2\lambda_y\gamma^2\left(1+A_6^2\right)B_5}{\pi^3A_5B_4} + \frac{4\lambda_x(1-\omega)^2A_7}{\gamma^2\pi A_5B_4} \tag{17}$$

$$\lambda_x = \frac{k_x a}{2D} \tag{18a}$$

$$\lambda_y = \frac{k_y b}{2D} \tag{18b}$$

The value of the critical elastic local buckling coefficient k_{cr} can be obtained by taking a partial derivative of Eq. (17) with respect to γ and setting the derivative equal

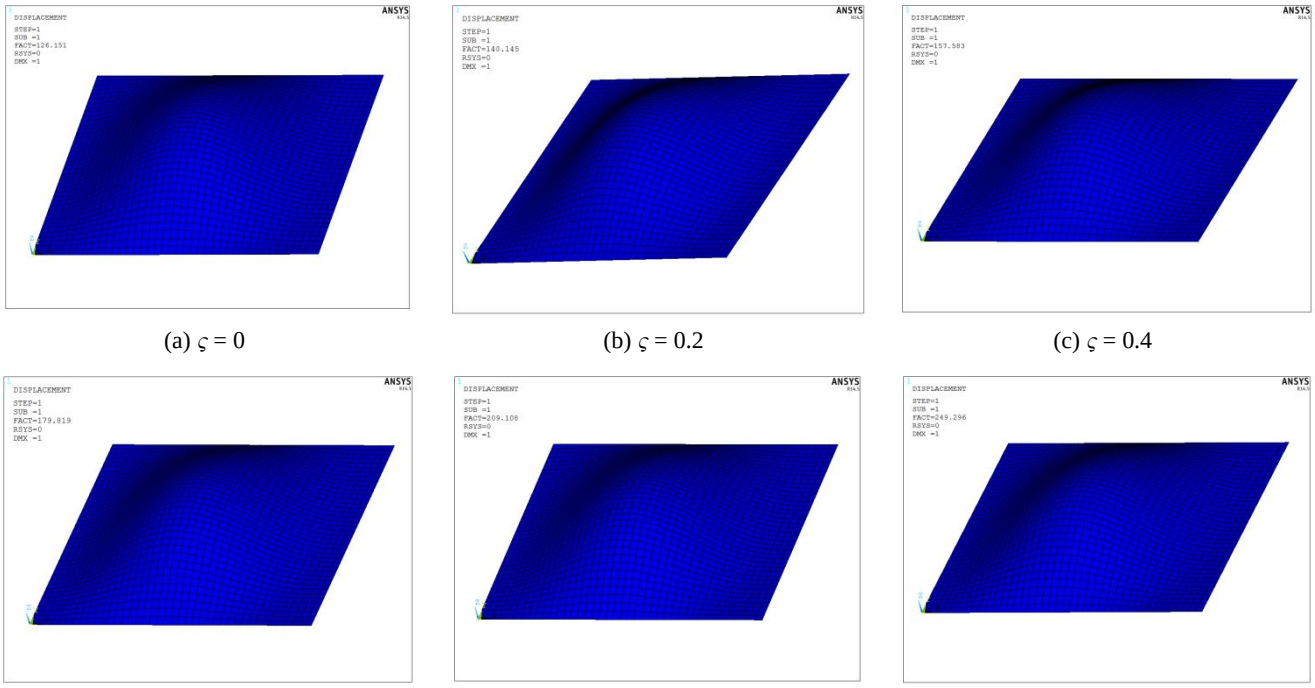

(a) $\varsigma = 0$ (b) $\varsigma = 0.2$ (c) $\varsigma = 0.4$

(d) $\varsigma = 0.6$ (e) $\varsigma = 0.8$ (f) $\varsigma = 1.0$

Fig. 3 Buckling shapes with different ω values

to zero. The corresponding critical aspect ratio γ_{cr} can be calculated by

$$\gamma_{cr} = \left[\frac{\pi^3 A_1 B_1 + 4\lambda_x \pi^2 (1-\omega)^2 A_7}{A_2 B_2 + 2\lambda_y (1+A_6^2) B_5} \right]^{\frac{1}{4}} \tag{19}$$

Inserting Eq. (19) into Eq. (17), the critical elastic local buckling coefficient k_{cr} can be determined. Then the critical local buckling stress of steel plate σ_{cr} is calculated by substituting k_{cr} and D into Eq. (16) as

$$\sigma_{cr} = \frac{k_{cr} \pi^2 E}{12(1-\nu^2)(b/t)^2} \tag{20}$$

3. Verification

In order to verify the proposed explicit solutions, two different approaches were used. Explicit solutions and numerical results by other researchers in the literature, and finite element results obtained by the commercial program ANSYS are compared in this section. The details of the finite element models could be referred to Qin *et al*. (2018). The brief information was listed below. The material properties of the steel plates considered are: $E = 2.06\times10^5$ N/mm^2, $\nu = 0.3$. In the modelling herein, the steel plate was modelled by the 8-node shell elements SHELL93, and the concrete was modelled by the 8-node solid structural elements SOLID65. The interface between steel plate and concrete was simulated by creating contact pairs with the 3-D target surface elements TARGE170 and the 3-D 8-node surface-to-surface contact elements CONTA174. The rotational restraints were modelled by a series of spring elements COMBIN14 connected to the nodes along the edges of steel plate.

3.1 Boundary condition 1: Clamped loaded edges and simply-supported unloaded edges (CS)

The steel plate with clamped loaded and simply-supported unloaded edges is represented by CS steel plate. The boundary condition of clamped loaded edges at $x = 0$ and a corresponds to $\omega = 1$, while that of simple supported unloaded edges at $y = 0$ and b corresponds to $\lambda_y = 0$. The value of critical aspect ratio $\gamma_{cr} = 1.52$ can then be obtained by Eq. (19). Substituting $\gamma_{cr} = 1.52$ into Eq. (17) gives the value of critical local buckling coefficient k_{cr} as

$$k_{cr} = \frac{5.467}{1-0.5\varsigma} \tag{21}$$

Particularly, $\varsigma = 0$ leads to $k_{cr} = 5.467$. This case is reduced to the research in Qin *et al*. (2017) and corresponds to the loading condition that the steel plate is subjected to uniform compression. This results is close to $k_{cr} = 5.6$ proposed by Uy and Bradford (1996) based on finite strip method, and $k_{cr} = 5.06$ given by Qin *et al*. (2018) according to the application of a different shape function.

For steel plate with different value of ς, the buckled shapes of a square steel plate with the aspect ratio $\gamma = 1$ obtained by the finite element simulations are shown in Fig. 3. The width and thickness of the steel plate are $b = 100$ mm and $t = 1$ mm, respectively. A comparison between the proposed explicit and finite element eigenvalue solutions is given in Table 1 and Fig. 4(a).

As indicated in Table 1 and Fig. 4(a), the explicit results agree well with the finite element results for the plates with

Table 1 Comparison of local buckling stress for CS steel plate

ς	Explicit N/mm^2	FE N/mm^2	Exp/FE	ς	Explicit N/mm^2	FE N/mm^2	Exp/FE
0	125.09	126.15	0.99	0.1	131.67	132.78	0.99
0.2	138.99	140.15	0.99	0.3	147.16	148.38	0.99
0.4	156.36	157.58	0.99	0.5	166.79	167.99	0.99
0.6	178.70	179.82	0.99	0.7	192.45	193.33	1.00
0.8	208.48	209.11	1.00	0.9	227.44	227.50	1.00
1.0	250.18	249.30	1.00				

clamped loaded edges and simply-supported unloaded edges. The maximum difference is about 0.84% between the finite element eigenvalue and the explicit solutions.

3.2 Boundary condition 2: *Clamped loaded and unloaded edges* (*CC*)

The steel plate with clamped both loaded and unloaded edges is represented by CC steel plate. The boundary condition of clamped loaded edges at $x = 0$ and a corresponds to $\omega = 1$, while that of clamped unloaded edges at $y = 0$ and b corresponds to $k_y \to \infty$. The value of critical aspect ratio $\gamma_{cr} = 1.0$ can then be obtained by Eq. (19). Substituting $\gamma_{cr} = 1.0$ into Eq. (17) gives the value of critical local buckling coefficient k_{cr} as

$$k_{cr} = \frac{10.31}{1-0.5\varsigma} \tag{22}$$

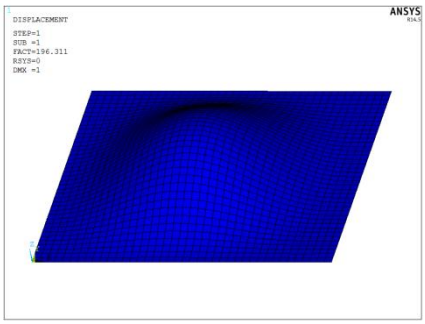

Fig. 5 Typical buckled shape of steel plate with clamped loaded and unloaded edges

Particularly, $\varsigma = 0$ reduces to the case studied by Qin *et al*. (2017) and means the steel plate is under uniform compression. It leads to $k_{cr} = 10.31$. This results is close to $k_{cr} = 10.12$ by Qin *et al*. (2018) based on a different function shape, $k_{cr} = 10.31$ proposed by Uy and Bradford (1996), and $k_{cr} = 10.312$ suggested by Long *et al*. (2016).

The typical buckled shape of a square steel plate with all edges clamped is obtained by the finite element method and is illustrated in Fig. 5. For square steel plate (b = 100 mm and t = 1 mm) with different values of ς, a comparison between the proposed explicit and finite element eigenvalue solutions is given in Table 2 and Fig. 4(b).

It can be observed from Table 2 and Fig. 4(b) that, in general, the formulas proposed has good accuracy with the numerical solutions. The ratios of the predicted explicit solutions to the numerical ones range from 1.08 to 1.10 with a mean of 1.08 and a standard deviation of 0.002. These values closely correspond.

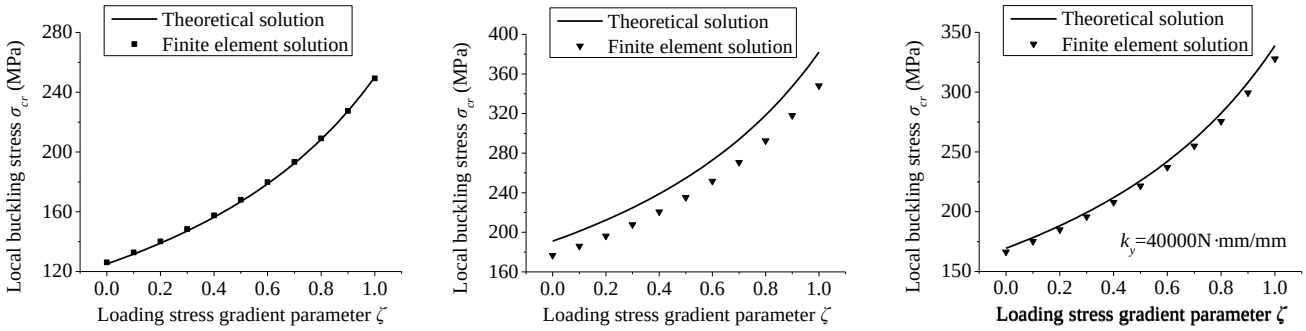

(a) For CS steel plate (b) For CC steel plate (c) For CK steel plate

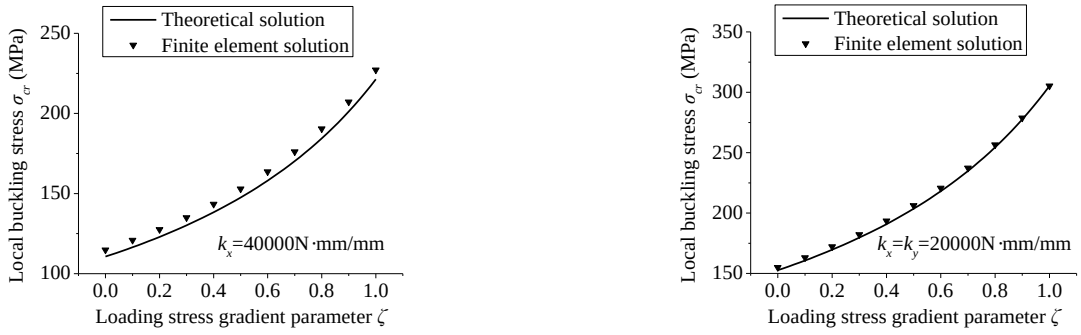

(d) ς = 0.6 (e) ς = 0.8

Fig. 4 Comparison of local buckling stress

Table 2 Comparison of local buckling stress for CC steel plates

ς	Explicit N/mm^2	FE N/mm^2	Exp/FE	ς	Explicit N/mm^2	FE N/mm^2	Exp/FE
0	191.07	176.73	1.08	0.1	201.12	186.02	1.08
0.2	212.30	196.31	1.08	0.3	224.78	207.77	1.08
0.4	238.83	220.64	1.08	0.5	254.75	235.20	1.08
0.6	272.95	251.73	1.08	0.7	239.95	270.66	1.09
0.8	318.44	292.49	1.09	0.9	347.39	318.04	1.09
1.0	382.13	348.11	1.10				

Table 3 Comparison of local buckling stress for CK steel plate

ς	Explicit N/mm^2	FE N/mm^2	Exp/FE	ς	Explicit N/mm^2	FE N/mm^2	Exp/FE
0	169.44	166.44	1.02	0.1	178.36	175.21	1.02
0.2	188.27	184.90	1.02	0.3	199.34	195.69	1.02
0.4	211.80	207.81	1.02	0.5	225.92	221.52	1.02
0.6	242.06	237.09	1.02	0.7	260.68	254.91	1.02
0.8	282.40	275.47	1.03	0.9	308.08	299.49	1.03
1.0	388.88	327.84	1.03				

Table 4 Comparison of local buckling stress for KS steel plate

ς	Explicit N/mm^2	FE N/mm^2	Exp/FE	ς	Explicit N/mm^2	FE N/mm^2	Exp/FE
0	110.67	114.80	0.96	0.1	116.49	120.86	0.96
0.2	122.96	127.52	0.96	0.3	130.19	134.98	0.96
0.4	138.33	143.38	0.96	0.5	147.55	152.91	0.96
0.6	158.09	163.64	0.97	0.7	170.25	176.09	0.97
0.8	184.44	190.43	0.97	0.9	201.21	207.21	0.97
1.0	221.33	227.16	0.97				

Table 5 Comparison of local buckling stress for KK steel plate

ς	Explicit N/mm^2	FE N/mm^2	Exp/FE	ς	Explicit N/mm^2	FE N/mm^2	Exp/FE
0	152.67	154.90	0.99	0.1	160.70	163.06	0.99
0.2	169.63	172.08	0.99	0.3	179.61	182.17	0.99
0.4	190.83	193.46	0.99	0.5	203.55	206.21	0.99
0.6	218.09	220.71	0.99	0.7	234.87	237.27	0.99
0.8	254.44	256.53	0.99	0.9	277.57	278.82	1.00
1.0	305.33	305.30	1.00				

3.3 Boundary condition 3: *Elastically restrained two opposite edges*

Normally, the restraint at the loaded edges is stiffer than that along the unloaded edges. Therefore, another two common cases usually applied are: (1) the steel plate is clamped at the loaded edges while elastically restrained along the unloaded edges (CK steel plate); (2) the steel plate is elastically restrained at the loaded edges and simply-supported along the unloaded edges (KS steel plate).

Finite element simulation was conducted by commercial program ANSYS. The standard springs connecting the boundary nodes to "rigid" support in different directions are chosen for the rotational restraining springs. The elastic rotational stiffness of springs is set as 40000 N·mm/mm.

For the steel plate with clamped loaded edges and elastically restrained unloaded edges (CK steel plate), the comparison between the proposed explicit and finite element eigenvalue solutions is given in Table 3 and Fig. 4(c). The averaged ratio of explicit solutions to finite element results is 1.02 and the standard deviation is 0.005.

For the steel plate with elastically restrained loaded edges and simply-supported unloaded edges (KS steel plate), the comparison between the proposed explicit and finite element eigenvalue solutions is given in Table 4 and Fig. 4(d). The averaged ratio of explicit solutions to finite element results is 0.96 and the standard deviation is 0.007.

3.4 Boundary condition 4: *Elastically restrained along both loaded and unloaded edges* (*KK*)

In order to verify the accuracy of the present explicit solution for steel plate with elastic restraints along four edges, eleven finite element models were established with the same material properties and geometry size of steel plate as described in the sections above. The elastic rotational springs of both loaded and unloaded edges were chosen as 20000 N·mm/mm. As indicated in Table 5 and Fig. 4(e), the present solutions of critical stress resultants compare closely with finite element eigenvalue analytical results. It can also be concluded that the present explicit solution is highly accurate and can be used with confidence in local buckling analysis.

4. Design recommendation

The model presented in this paper is based, for most part, on sound engineering principles. It is important, though, to stress at this point that simplifications and assumptions should be made to both reduce the model's complexity to a reasonable level and contribute for practical design.

For a more general case where the CFT column is under combined bending and axial compression in practical engineering application, it is of significance to determine the values of k_x and k_y to obtain the explicit solution for steel plates with both loaded and unloaded edges elastically restrained. Normally the loaded edges of the steel plate can be regarded as be clamped while the unloaded edges is more exactly to consider elastically rotationally restraint, i.e., it can be assumed that $k_x \rightarrow \infty$. In this case and referring back to Eq. (17), the most important issue to deal with is to find out the most suitable solutions for λ_y. Based on the research by Bleich and Qin *et al*. (2017), modified equations to predict the elastically restraining factor for

steel plate in concrete filled tubular columns are given in Eqs. (23)-(25) (Qin *et al*. 2017).

$$\lambda_y = \left(\frac{t_w}{t_f}\right)^3 \frac{r}{\rho} \tag{23}$$

$$r = 1 - \beta_r \left(\frac{t_f b_w}{t_w b_f}\right)^2 \tag{24}$$

$$\rho = \frac{1}{\pi}\tanh\left(\frac{\pi b_w}{4b_f}\right)\left[1 + \frac{\pi b_w / 2b_f}{\sinh\left(\pi b_w / 2b_f\right)}\right] \tag{25}$$

where b_f and t_f are the width and thickness of the calculated steel plate, respectively; b_w and t_w are the width and thickness of the adjacent steel plate, respectively. β_r = 0.5 is the reduction factor used for considering the beneficial restraining effects offered by concrete.

The simplification and assumption made in this section should be verified by test results. However, there is a dearth of information for experimental data of local buckling of steel plates under combined bending and compression. Therefore, the test data of local buckling of CFT columns under axial compression (ς = 0) from Uy (2001) and Mo *et al*. (2004) are compared with the calculated ones by the proposed model, as an indirect way to calibrate the proposed theoretical model. The comparison results are given in Table 1 of Qin *et al*. (2017).

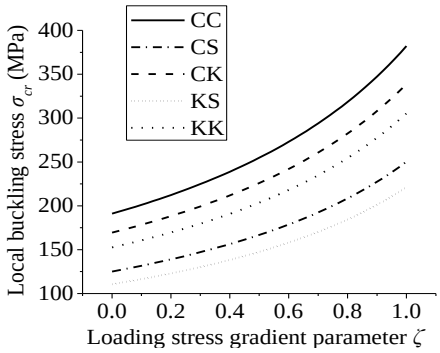

Fig. 6 Relationship between local buckling stress and loading stress gradient parameter

5. Parametric study

As can be observed from Eq. (17), the explicit critical local buckling coefficient is a function of the loading stress gradient parameter ς, the aspect ratio γ, and the rotational restraint stiffness k_x and k_y. A parametric study is conducted to evaluate the effects of these three parameters on the local buckling stress resultants of steel plates.

5.1 Loading stress gradient parameter ς

The relationship between the local buckling stress and the loading stress gradient parameter is plotted in Fig. 6. For a fixed aspect ratio γ = 1.0, as expected, the steel plate with elastically restrained loaded edges and simply-supported unloaded edges (KS) has the lowest local buckling stress, while the steel plate with clamped both loaded and unloaded edges has the highest one. The minimum value of the local bucking stress of steel plate with different

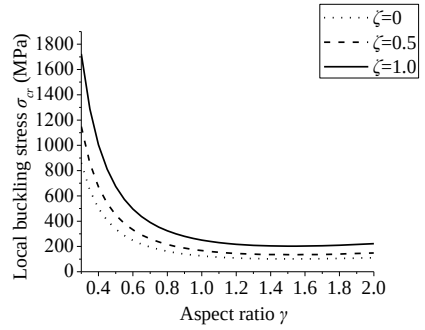

(a) For CS steel plate

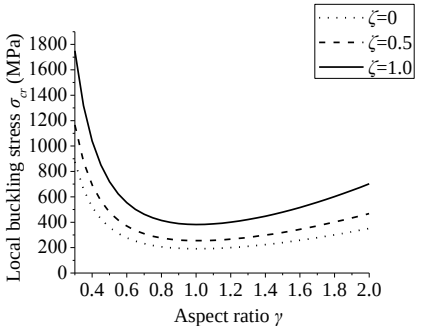

(b) For CC steel plate

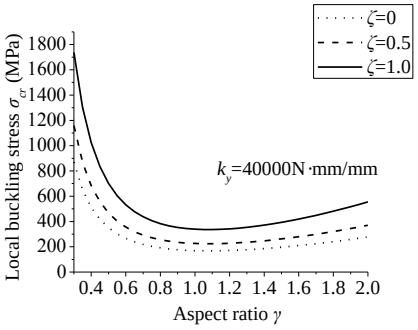

(c) For CK steel plate

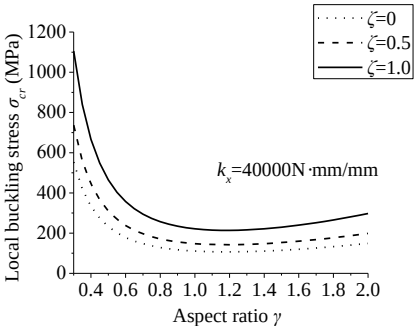

(d) For KS steel plate

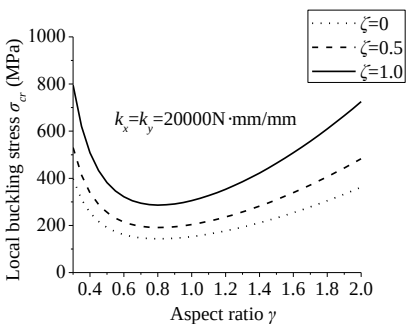

(e) For KK steel plate

Fig. 7 Relationship between local buckling stress and aspect ratio

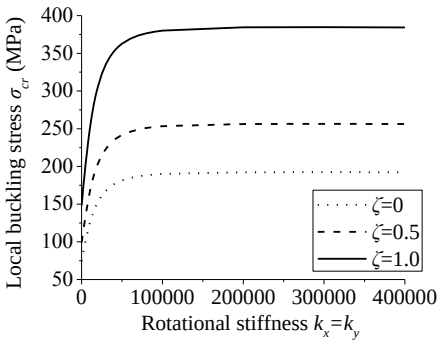

Fig. 8 Relationship between local buckling stress and rotational stiffness

boundary conditions can be obtained when the loading stress gradient parameter ς = 0. This indicates that the square steel plate is more vulnerable to local buckling when it is subjected to uniform axial compression, which is consistent to the conclusion by Qin *et al*. (2018).

5.2 Aspect ratio γ

The relationship between the local buckling stress of steel plate with different boundary conditions and the aspect ratio is plotted in Fig. 7. The buckling stress of CS steel plate reaches the minimum value when the aspect ratio approaches 1.5 as shown in Fig. 7(a), while for CC steel plate, the minimum value of buckling stress is reached when the aspect ratio approaches 1.0, as indicated in Fig. 7(b). Furthermore, the steel plates under eccentric compression (ς = 1.0) are slightly more sensitive to the change of the aspect ratio than under uniform compression (ς = 0).

5.3 Rotational restraint stiffness k_x and k_y

The buckling stress are plotted with respect to the rotational stiffness ($k_x = k_y$) in Fig. 8, for a given aspect ratio γ = 1.0. As expected, the buckling stress of the square steel plates increases with the growth of the rotational stiffness. The buckling stress is almost proportional to the rotational stiffness when the rotational stiffness is low. On the other hand, when the rotational stiffness becomes relatively large (close to the clamped boundary), the influence of the increase in the rotation stiffness on the buckling stress is negligible. Furthermore, the steel plate with ς = 1.0 is the most sensitive to the change of the rotational stiffness, while the steel plate subjected to uniform compression (ς = 0) is the least sensitive to be influenced by the change of the rotational stiffness.

6. Conclusions

In this study, Rayleigh-Rize approach, which assembles the method used by Qin *et al*. (2017, 2018), is used to establish the eigenvalue problem for the local buckling behavior of steel plates elastically restrained along its four edges and subjected to combined bending and compression. Buckling shape functions combining trigonometric and biquadratic functions, which have been used by Qin *et al*. (2017) to study the case of uniform compression, are introduced to obtain the explicit solution. The derived solutions for steel plates with elastically restrained edges are simplified to several special cases based on the different edge restraining conditions (e.g., simply-supported, clamped, or rotationally restrained). Validity of the explicit solutions presented is demonstrated by a good agreement of comparison to available explicit solutions in the literature, and finite element results. A parametric study is further conducted to investigate the influences of the loading stress gradient parameter, the aspect ratio, and the rotational restraint stiffness on the local buckling stress resultants of steel plates with different boundary conditions. This research extends the work by Qin *et al*. (2017) to the case of steel plate under eccentric compression and can also indirectly verify the accuracy of research by Qin *et al*. (2018) by using a different shape function to obtain the local buckling solution.

Acknowledgments

This work is sponsored by the Natural Science Foundation of Jiangsu Province (Grant No. BK20170685), the National Key Research and Development Program of China (Grant No. 2017YFC0703802), the National Natural Science Foundation of China (Grant No. 51808117), the state Key Laboratory of Subtropical Building Science, South China University of Technology, China (Grant No. 2018ZB26), and the Fundamental Research Funds for the Central Universities (Grant No. 2242018K40137).

References

Abbasi, M., Khezri, M., Rasmussen, K.J.R. and Schafer, B.W. (2018), "Elastic buckling analysis of cold-formed steel built-up sections with discrete fasteners using the compound strip method", *Thin-Wall. Struct.*, **124**, 58-71.

Burgos, C.A., Jaca, R.C. and Godoy, L.A. (2018), "Post-buckling behavior of fluid-storage steel horizontal tanks", *Int. J. Press. Ves. Pip.*, **162**, 46-51.

De Holanda, A.S. and Gonçalves, P.B. (2003), "Postbuckling Analysis of Plates Resting on a Tensionless Elastic Foundation", *J. Eng. Mech.*, **129**(4), 438-448.

Dong, J.H., Ma, X., Zhuge, Y. and Mills, J.E. (2017), "Shear buckling analysis of laminated plates on tensionless elastic foundations", *Steel Compos. Struct., Int. J.*, **24**(6), 697-709.

Dong, J.H., Ma, X., Zhuge, Y. and Mills, J.E. (2018), "Unilateral contact buckling behaviour of orthotropic plates subjected to combined in-plane shear and bending", *Int. J. Solids Struct.*, **150**, 135-153.

Fang, C., Yam, M.C.H., Lam, A.C.C. and Ke, K. (2017), "Reinforcing strategies for double-coped beams against local web buckling", *Eng. Struct.*, **152**, 736-749.

Gheidi, A., Mirtaheri, M., Zandi, A.P. and Alanjari, P. (2011), "Effect of filler material on local and global behaviour of buckling-restrained braces", *Struct. Des. Tall Spec. Build.*, **20**(6), 700-710.

Klouche, F., Darcherif, L., Sekkal, M. and Tounsi, A. (2017), "An original single variable shear deformation theory for buckling analysis of thick isotropic plates", *Struct. Eng. Mech., Int. J.*, **63**(4), 439-446.

Li, D., Smith, S. and Ma, X. (2016), "End condition effect on initial buckling performance of thin plates resting on tensionless elastic or rigid foundations", *Int. J. Solids Struct.*, **105**, 83-89.
Liu, D.Y., Liu, H.B., Chen, Z.H. and Liao, X.W. (2017), "Structural behavior of extreme thick-walled cold-formed square steel tube", *J. Constr. Steel Res.*, **128**, 371-379.
Liu, Z.A., Liu, H.B., Chen, Z.H. and Zhang, G.P. (2018), "Structural behavior of cold-formed thick-walled rectangular steel columns", *J. Constr. Steel Res.*, **147**, 277-292.
Long, Y.L., Wan, J. and Cai, J. (2016), "Theoretical study on local buckling of rectangular CFT columns under eccentric compression", *J. Constr. Steel Res.*, **120**, 70-80.
Ma, X., Butterworth, J. and Clifton, C. (2008), "Initial compressive buckling of clamped plates resting on tensionless elastic or rigid foundations", *J. Eng. Mech.*, **134**(9), 514-518.
Mirtaheri, M. and Zoghi, M.A. (2016), "Design guides to resist progressive collapse for steel structures", *Steel Compos. Struct., Int. J.*, **20**(2), 357-378.
Mirtaheri, M., Sehat, S. and Nazeryan, M. (2018), "Improving the behavior of buckling restrained braces through obtaining optimum steel core length", *Struct. Eng. Mech., Int. J.*, **65**(4), 401-408.
Mo, S., Zhao, R. and Zhong, X. (2004), "Local buckling research on concrete filled square steel box member", *J. Hunan U. Sci. Tech.* (Natural Science Edition), **19**, 43-47.
Naghsh, A., Azhari, M. and Saadatpour, M.M. (2018), "Thermal buckling analysis of point-supported laminated composite plates in unilateral contact", *Appl. Math. Model.*, **56**, 564-583.
Patton, M.L. and Singh, K.D. (2017), "Buckling of fixed-ended concrete-filled steel columns under axial compression", *Int. J. Steel Struct.*, **17**(3), 1059-1071.
Qiao, P., Chen, F., Xu, J. and Lu, Z. (2013), "Local buckling analysis of restrained orthotropic plates under generic in-plane loading", *J. Eng. Struct.*, 1**39**(8), 936-951.
Qin, Y., Chen, Z.H., Bai, J.J. and Li, Z.L. (2016), "Test of extended thick-walled through-diaphragm connection to thick-walled CFT column", *Steel Compos. Struct., Int. J.*, **20**(1), 1-20.
Qin, Y., Lu, J.Y. and Cao, S. (2017), "Theoretical study on local buckling of steel plate in concrete-filled tube column under axial compression", *ISIJ Int.*, **57**(9), 1645-1651.
Qin, Y., Du, E.F., Li, Y.W. and Zhang, J.C. (2018), "Local buckling of steel plates in composite structures under combined bending and compression", *ISIJ Int.*, **58**(11).
DOI: https://doi.org/10.2355/isijinternational.ISIJINT-2018-202
Shen, H.S. and Li, Q.S. (2004), "Postbuckling of shear deformable laminated plates resting on a tensionless elastic foundation subjected to mechanical or thermal loading", *Int. J. Solids Struct.*, **41**(16-17), 4769-4785.
Thai, H.T., Kim, S.E. and Kim, J. (2017), "Improved refined plastic hinge analysis accounting for local buckling and lateral-torsional buckling", *Steel Compos. Struct., Int. J.*, **24**(3), 339-349.
Uy, B. (2001), "Local and postlocal buckling of fabricated steel and composite cross sections", *J. Struct. Eng.*, **127**(6), 666-677.
Uy, B. and Bradford, M.A. (1996), "Elastic local buckling of steel plates in composite steel-concrete members", *Eng. Struct.*, **18**(3), 193-200.
Villarreal, E. and Abajo, D. (2018), "Buckling and modal analysis of rotationally restrained orthotropic plates", *Progress Aerosp. Sci.*, **78**, 116-130.
Wright, H.D. (1993), "Buckling of steel plates in contact with a rigid medium", *Struct. Engr.*, **71**(12), 209-215.
Yerudkar D.S. and Vesmawala, G.R. (2018), "Strength and buckling of cold-formed steel laterally unbraced stiffened C and Z sections", *P. I. Civil Eng.-Str. B.*, **171**(3), 216-225.